



HAL
open science

Modeling and analysis of concentration profiles obtained by in-situ SAXS during cross-flow ultrafiltration of colloids

Y. Jin, N. Hengl, S. Baup, G. Maitrejean, F. Pignon

► **To cite this version:**

Y. Jin, N. Hengl, S. Baup, G. Maitrejean, F. Pignon. Modeling and analysis of concentration profiles obtained by in-situ SAXS during cross-flow ultrafiltration of colloids. *Journal of Membrane Science*, 2017, 528, pp.34-45. 10.1016/j.memsci.2017.01.019 . hal-02006323

HAL Id: hal-02006323

<https://hal.science/hal-02006323>

Submitted on 29 Aug 2022

HAL is a multi-disciplinary open access archive for the deposit and dissemination of scientific research documents, whether they are published or not. The documents may come from teaching and research institutions in France or abroad, or from public or private research centers.

L'archive ouverte pluridisciplinaire **HAL**, est destinée au dépôt et à la diffusion de documents scientifiques de niveau recherche, publiés ou non, émanant des établissements d'enseignement et de recherche français ou étrangers, des laboratoires publics ou privés.

Modeling and analysis of concentration profiles obtained by in-situ SAXS during cross-flow ultrafiltration of colloids

Y. Jin ^{a,b}, N. Hengl ^{a,b*}, S. Baup ^{a,b}, G. Maitrejean ^{a,b}, F. Pignon ^{a,b*}

^a Univ. Grenoble Alpes, LRP, F-38000 Grenoble, France

^b CNRS, LRP, F-38000 Grenoble, France

Abstract

Concentration profiles and structural organization of different colloidal suspensions in the vicinity of membrane during ultrasonic-assisted ultrafiltration were previously evidenced from non-destructive, real-time, *in-situ* SAXS measurements [Jin *et al.*, J. Membr. Sci. 453 (2014) 624–635][Jin *et al.*, J. Membr. Sci. 470 (2014) 205–218]. On the basis of these obtained results, this paper explored by numerical calculation, four key factors of the buildup of concentrated polarization layer in such process (matter accumulation, flow property, permeability and osmotic pressure). Two different kind of systems have been studied: anisotropic Laponite clay particles and soft casein micelle particles. For all the systems and filtration conditions investigated, the results have shown that the level of matter accumulated is directly linked to calculated permeation flux and in accordance with the experimental one. The rheological parameters introduced in the calculations have allowed to deduce the charts of yield stress in the concentrated layers and revealed the important role of suspensions flow properties in the mechanisms of filtration involved near the membrane surface. The measured properties of the accumulated layers have been computed with a recent model based upon permeability and osmotic pressure [Bouchoux *et al.*, Langmuir. 30 (2013) 22–34]. It has been shown good agreement between modeled and experimental values in permeation flux for all the different systems and filtration explored.

Keywords: *cross-flow ultrafiltration, fouling, SAXS, skim milk, colloid, ultrasound*

* Corresponding authors: frederic.pignon@ujf-grenoble.fr, nicolas.hengl@ujf-grenoble.fr

1. INTRODUCTION

Cross-flow ultrafiltration of colloids is mainly limited by matter accumulation on the membrane surface, as majority of membrane processes. The events leading to the formation of a concentrated layer close to the membrane surface are taking place at a length scale of nanometers. Indeed, the interactions between the particles at this scale are very important, which requires an understanding of colloidal interactions during such process. Originating from various forces, colloidal interactions are responsible for strikingly influencing the transport properties of colloidal suspensions, such as gradient diffusivity, flow properties and the thermodynamic properties such as the osmotic pressure [1]. Those characteristics are considered to play important roles in the process of ultrafiltration of colloids. As a result, considerable research effort has been devoted to understand this process by taking into account them appropriately [2–10]. However, understanding of cross-flow ultrafiltration is not yet complete so far. Modeling of this process has been studied since twenty years, several approaches have been proposed with a global approach [1-10]. In fact, what is desperately required for both modeling and fundamental understanding of the process is an accurate local characterization that is non-destructive, and which can provide real-time, *in-situ* observation of the concentrated particle layers during filtration. Fortunately, our previous works have offered us these desired results by Small-Angle X-ray Scattering (SAXS) measurements. Colloids of different physico-chemical properties, of both model anisotropic nanometric hard discs of clay particles and naturally soft casein micelles particles, have been investigated. Their concentration profiles and the structural organizations in the vicinity of membrane during ultrasonic assisted filtration have been characterized by non-destructive, real-time, *in-situ* SAXS measurements and for different operating filtrations conditions [11–14].

Consequently, the main goal of this paper is to describe the relationships between the measured and/or calculated permeation flux, and the mechanical and structural properties of accumulated concentrated layers. The results on concentration profile and properties of accumulated layers, offer the possibility to give some predictions by numerical calculations, in order to better understand the mechanisms involved in the filtration process. The principal questions addressed are: what is the quantity of matter accumulated? what are the levels of stresses, osmotic pressure and permeability in these accumulated layers? which are the correlations between the mechanical and structural properties of the accumulated layers, and the filtration performance (permeation flux)? Is there a spatial distribution of matter accumulation along the membrane surface as reported before [15,16], and how does it affect the permeation flux?

Furthermore, some results on the effect of ultrasound (US) on the properties of concentrated layers have been obtained. It allowed the possibility to explore the time dependent equilibrium phenomena involved in the growth or disruption of concentrated layers. The extent of the internal cohesive forces

of the accumulated layers has to be compared to the external forces induced by the combine effect of the cross- flow and shearing phenomena associated to the US.

Finally, an assessment of theoretical model proposed by Bouchoux *et al.* [17] has been performed with our obtained concentration profiles for different colloids. This aspect aims to, firstly, predict the permeate flux along the membrane; secondly, examine the reliability of two key factors involved in this model: permeability and osmotic pressure of concentrated layer.

2. MATERIALS AND METHODS

2.1 Investigated suspensions

This paper mainly involves two colloidal suspensions:

Laponite XLG suspensions, from Laponite Industry, is made of nanometric platelets with an average lateral dimension of 30 nm and 1 nm in thickness, and is used with or without tetrasodium diphosphate $\text{Na}_4\text{P}_2\text{O}_7$ (tspp) as a peptizer (6 % with regard to dry clay mass) [11].

The dispersions were prepared under high shear in a solution of distilled water (10^{-3} M NaCl) at 20°C. The dispersions were then aged in closed vessels for 12 days before the filtration experiments. The pH value of the dispersions remained stable during this aging time and equal to 10 during the measurement. Dispersions to be filtered were prepared at initial volume fractions of $\phi_v = 0.48\%$ and 1%, corresponding to mass fraction of 0.0121 g.cm³ and 0.0253 g.cm³, respectively. The structure and rheology of colloidal suspensions of Laponite have been extensively studied in our precedent works [18-22]. Scattering studies indicate that, for ionic strengths and pH domain identical of the one used in this work, the Laponite particles attract each other in edge-to-face configurations [21]. This causes the particles to gather in micro-domains, which subsequently associate to form fractal aggregates. A gel results when the network of connections spans the sample. This network is destroyed by the application of sufficient strain, and as a result, the viscosity of Laponite suspensions decreases under shear [22]. Above a critical volume fraction which defines the sol-gel transition and for identical physico-chemical conditions (ionic strength and pH) as those of the samples we studied here, Laponite suspensions form a thixotropic gel. In order to control the electrostatic particle interaction some peptizer (tetrasodium diphosphate $\text{Na}_4\text{P}_2\text{O}_7$) has been added to the suspension. In our precedent works it has been shown that the diphosphate anion binds the positive surface charge of the edges of the platelets. This has the consequence to reduce the strength of edge-face and edge-edge attractions between the particles. The result of this reduction in attractive forces between the particles is a partial disruption of the network which induce a decrease in viscosity and yield stresses in the gel [18-22]. To

simplify the text, the two used samples for filtration will be denoted by Lap0.48-tspp6 ($\phi_v = 0.48$ %, addition of tspp: 6%) and Lap1-tspp0 ($\phi_v = 1$ %, no addition of tspp). In the discussion, the term “Lap-tspp0” or “Lap-tspp6” will be also used to denote the pure Laponite dispersions or those containing peptizers without regard to the volume fraction. The initial filtration volume fraction is denoted ϕ_{v0} .

Skim milk suspensions: they were prepared from ‘Low Heat’ Bovine Skim Milk Powder containing soluble proteins and mineral salts in addition to casein micelles, the major protein of milk. This powder was provided by “UMR 1253 INRA Agrocampus Ouest, STLO Science et Technologie du Lait et de l’Œuf” Rennes, France [12]. To prevent the development of bacteria, sodium azide (0.2 g.L^{-1}) was added to the suspension. The casein micelle content of standard skim milk suspension is about $C_0 = 27 \text{ g.L}^{-1}$ (26 g.kg^{-1}). To simplify the interpretation of results, a relative concentration C/C_0 was presented in this paper, where C is the casein micelle concentration of sample suspension (within concentrated layer at the membrane surface) and C_0 corresponds to the casein micelle concentration of standard skim milk (27 g.L^{-1}). Two initial filtration concentration were explored C_0 or $2x C_0$.

Casein micelle structural organization and rheological properties have been studied in details in previous works [12, 23,24]. Native casein micelles in milk are complex macromolecular assemblies composed of four distinct type of caseins, namely α_s1 , α_s2 , β and κ , as well as minerals, essentially calcium and phosphate called colloidal calcium phosphate (CCP). In milk, the native casein micelles are in equilibrium with an aqueous phase comprising whey proteins, a low content of soluble caseins and dissolved salts. Previous results obtained by SAXS revealed two characteristic length scales for the equilibrium structure of casein micelle with radius of gyration R_g , about 100 nm and 5.6 nm pertaining to the globular micelles and their non-globular internal structure, respectively [23]. The rheological behaviour of casein micelles as a function of concentration has been also studied in the past by conventional rheometric measurements [12] and rheo-SAXS measurements [23]. The rheological behavior follow an evolution at increasing concentration from Newtonian to shear-thinning (critical concentration $C = 108 \text{ g.L}^{-1}$) until the emergence of yield stress with the increase of concentration (sample concentration from 189 g.L^{-1} to 216 g.L^{-1}). The structural organization under shear has also been evaluated by rheo-SAXS and have allowed to show that even at high shear rate of 1000 s^{-1} at 25°C , the structural organization of the casein micelles is not modified.

2.2 Experimental set-up

The filtration device was previously described [11–14]: the custom ‘‘SAXS Cross-Flow US-coupling Filtration Cell’’ has a filtration channel with a dimension of 100 mm \times 4 mm \times 8 mm (length \times width \times height) which is combined with a sonotrode generating 20 kHz ultrasonic waves at an intensity of 0.6 to 2.9 W.cm⁻². In this paper, the applied ultrasound was 2 W.cm⁻². Flat polyethersulfone ultrafiltration membranes (PES 100 kDa, Pleiade®, Orelis Environnement, France) were used.

The SAXS measurements have been carried out at the ID02 High Brilliance Beamline [25], at the European Synchrotron Radiation Facility (ESRF), Grenoble, France. The measurement conditions and analytical methods have also been elaborately described [11–13]. Three windows are embedded into the wall located upstream ($x = 7$ mm), in the middle ($x = 50$ mm) and downstream ($x = 93$ mm) in the feed compartment (Fig. 1). The incident X-ray beam passes through the windows and interacts with the colloidal sample inside; the 2D scattered patterns of this beam are then recorded with a high-resolution CCD detector. These 2D patterns are normalized and radial averaged to obtain the scattering intensities. In precedent works, for specific x-ray beam intensity, the acquisition time were systematically studied and adapted in order to avoid any radiation damage of the particles. To asses that no radiation damage has occurred, several successive acquisitions at one exposure time were performed. The exposure time was reduced step by step until no change in the scattering intensity of two successive acquisitions is obtained. In all the cases at different concentrations or volume fractions studied no changes in the scattering intensity were detected for the shorter exposure times used. Furthermore, as the colloidal suspensions are submitted to a flow in the filtration cell, this reduces the potential appearance of a radiation damage. The scattering intensity profiles then serve to determine the sample concentrations as a function of distance from the membrane surface z , with an established calibration curve. Concentration profiles at the membrane surface are then deduced by gathering all the measured concentration points within the concentrated layer.

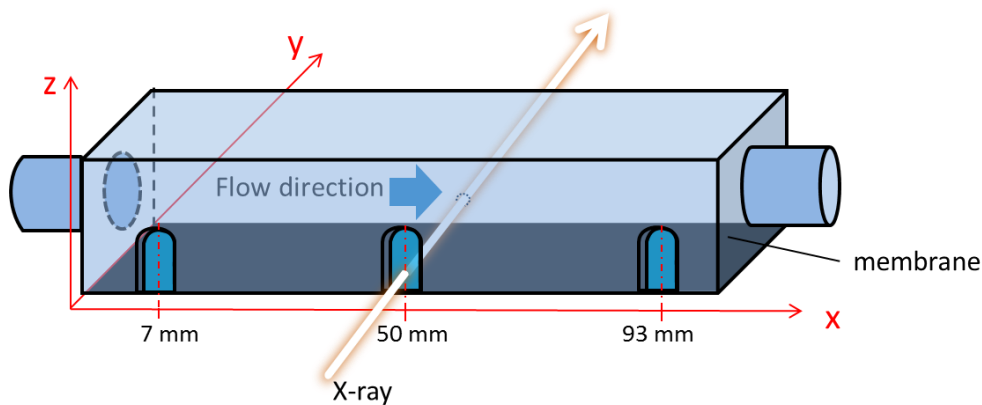


Fig. 1 Schematic view of the designed filtration cell

2.3 Numerical investigation

Colloidal suspensions of different physico-chemical properties have been investigated previously. Concentration profiles of filtrated suspensions at steady and transient states have been deeply discussed. In order to provide a global vision of process performance so as to reveal the general mechanism of concerned process, results obtained by SAXS measurements have been further analyzed by integrated calculations. Matlab software was used to carry out these calculations. This paper focuses on Laponite dispersions [11] and skim milk [12] since they represent different colloidal families which exhibit disparate filtration performance in ultrasonic-assisted cross-flow ultrafiltration.

We are interested in matter accumulation as well as the yield stresses of different z positions of concentrated particle layer. A theoretical model has also been used to predict the local permeate flux along the membrane surface [17]. The used model takes into account two principal factors: permeability and osmotic pressure of concentrated layer. Therefore, four key factors related to the buildup of concentrated particle layer have been investigated in this paper: matter accumulation, flow property, permeability and osmotic pressure.

2.3.1 Build-up of data matrix

Three windows of the filtration cell provide us the concentration profiles of suspension at three positions (vectors) along the membrane: at inlet ($x = 7$ mm), at the middle ($x = 50$ mm) and at outlet ($x = 93$ mm) of the filtration cell. The minimum distance above the membrane surface for obtaining exploitable SAXS data is $20\ \mu\text{m}$. Since exponential law of concentration profiles have been expected (as interpreted in Ref.[11]), an extrapolation by exponential law was firstly executed to complete the concentration profiles, as shown in Fig. 2.

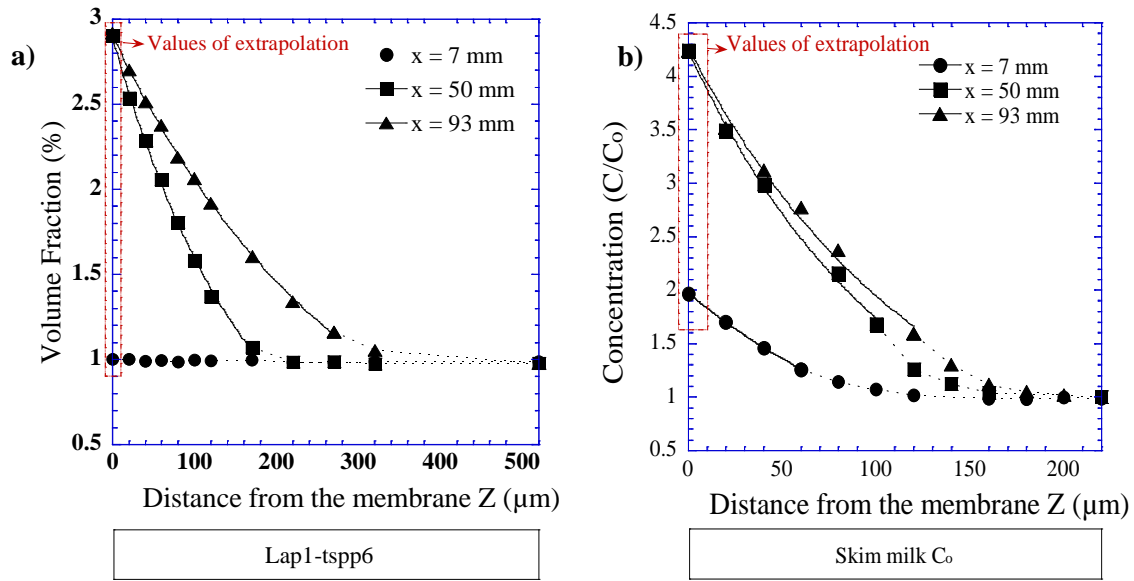


Fig. 2 Examples of data extrapolation by exponential law for the concentration profiles upstream, in the middle and downstream of filtration channel, at steady state. a) Lap1-tsp6, data extracted from Fig.12 of Ref. [11]: $T = 25 \pm 1^\circ\text{C}$, $\text{TMP} = 1.1 \times 10^5 \text{ Pa}$, $Q_v = 0.3 \text{ L.min}^{-1}$, without US; b) Skim milk ($C = C_0$), data extracted from Fig.11 of Ref.[12]: $T = 25 \pm 1^\circ\text{C}$, $\text{TMP} = 1.1 \times 10^5 \text{ Pa}$, $Q_v = 0.3 \text{ L.min}^{-1}$, without US. Solid lines correspond to exponential fits.

In order to execute the desired analysis, an appropriate interpolation is required. In this study, a linear interpolation was applied and a matrix of 51×86 (z axis \times x axis) was constituted with the help of Matlab software. Fig. 3a shows an example of the obtained chart of filtration channel (beyond $z = 1000 \mu\text{m}$) after this operation. Every single mesh of this figure corresponds to an infinitesimal box arising from the discretization of concentration profile. Then, for certain calculations such as matter accumulation or prediction of permeate flux, only concentrated layer was taken into account, bulk part was thus excluded. The position of the cut-off between bulk and matter is decided to be at the initial filtration volume fraction (Laponite) or the initial filtration concentration (milk). As shown in Fig. 3b, instead of feed concentration ($\phi_v = 1\%$ in this case), a value of zero was given to the bulk part. This operation allows not only excluding the effect of bulk part in the concerned calculations but also defining the thickness of concentrated layer and boundary layer of integrations presented later in this paper. These two charts are plotted for all the investigated situations; they are the bases of calculations in this paper.

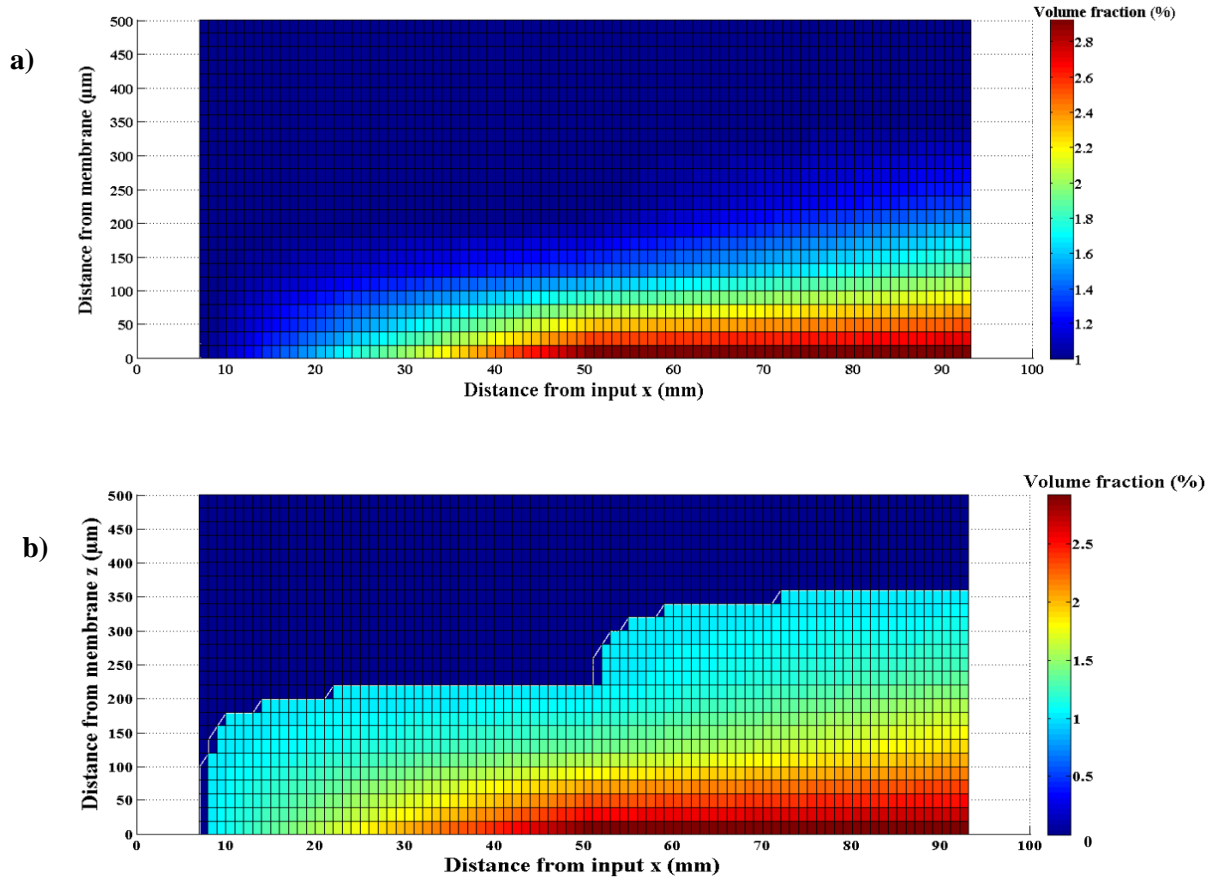


Fig. 3 Example of filtration channel charts. a) after data extrapolation and interpolation; b) after a further exclusion of bulk part. Data source: Lap1-tspp6, extracted from Fig.12 of Ref. [11]; $T = 25 \pm 1^\circ\text{C}$, $\text{TMP} = 1.1 \times 10^5 \text{ Pa}$, $Q_v = 0.3 \text{ L}\cdot\text{min}^{-1}$, without US.

2.3.2 Calculation of matter accumulation of concentrated layer

As described before, a matrix was established providing the concentration information of mapping points (particle density of infinitesimal boxes) within the filtration cell as function of x (along the membrane) and z (above the membrane). A triple integral of these infinitesimal boxes of concentration ($\text{g}\cdot\text{m}^{-3}$) over a three-dimensional region in xyz -space arises in the computation of mass, as denoted:

$$\text{mass} = \iiint C(x, y, z) dx dy dz \quad \text{Eq. 1}$$

Where $C(x,y,z)$ is the suspension concentration which is as function of spatial vectors (x, y, z) , as illustrated in Fig. 4. A numerical integral was then carried out so that matter accumulation of each infinitesimal column (vector) can be plotted along x -axis. This integral was achieved step by step. Firstly, a numerical integral by trapezoidal rule of $C(x,y,z)$ in the concentration- z plane was carried out.

The integration region is bounded by the curve $C(z)$ at given x , the z -axis and two vertical lines $z = 20 \mu\text{m}$ (the closest position from the membrane) and the first position where the concentration begins to be higher than feed suspension. The second vertical boundary line is also considered as the beginning of the concentrated layer, which defines its thickness δ . Accumulated mass of each infinitesimal column was then calculated by multiplying $\int_0^\delta c(x, y, z) dz$ with dx and Δy , with an assumption that there is no evolution of concentration along the y -axis. So far, matter accumulation can be plotted along x -axis. The mass of each infinitesimal column was then summed up to obtain the total mass of investigating concentrated layer.

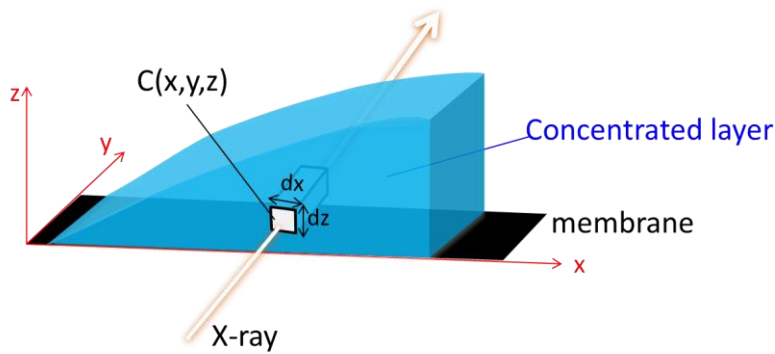


Fig. 4 Schematic of concentrated layer on the membrane surface

2.3.3 Build-up of shear stress charts of concentrated layer

Based upon the concentration profiles along the membrane (shown in Fig. 3), yield stress charts were plotted in the light of the dependence between yield stress (τ_o) and volume fraction (ϕ) for different suspensions: $\tau_o(\phi)$.

In order to get this $\tau_o(\phi)$, Laponite dispersion samples (ϕ from 1 % to 3 %) have been specifically prepared. Their flow properties of different state (at rest and after ultrasonic treatment) have been investigated (shown in Fig. 9). Two series of samples were prepared: one with 6 % of peptizer (tspp) and the other without it. Steady-state flow properties at 25 °C were then characterized by rheological measurements with shear rate controlled rheometers (DHR3, TA Instrument, France). Cone and plate geometries were employed (diameter 49 mm, angle 4°21'), whose surfaces were covered with sandpaper with a roughness of 200 μm in order to avoid sample slip at the geometry wall.

Effect of US on intact Laponite dispersions was also characterized. US treatment was exerted using the designed blade for filtration cell [11–14]. 20 ml of prepared Laponite samples were gently laid in a

100 mL rectangle container. US treatment (20 kHz, 2 W.cm⁻²) lasted 5 min (the residence time during real filtration). Then this sonicated sample was studied on the rheometer around 5 min after the US-treatment.

With the obtained τ_o/ϕ dependence for Laponite dispersions (which will be presented in section 3.2), the related yield stress of dispersion at each infinitesimal box can be calculated, which finally gave us the chart of yield stress of the concentrated layer within the filtration channel.

2.3.4 Prediction of permeate flux along the membrane

2.3.4.1 Model

In the basis of Darcy's law upon the concentrated layer (polarized layer and deposit), Bouchoux *et al.* [17] have recently published a dead-end filtration model taking into account the concentration (C, g.L⁻¹) dependence of both osmotic pressure (Π , Pa) and permeability (k_p , m²) of concentrated layer. The key equation of their model was:

$$J = - \frac{k_p(c)}{\eta} \frac{d\Pi(c)}{dz} \quad \text{Eq. 2}$$

With η the dynamic viscosity (Pa.s) of the solvent (permeate). Based upon two measurable parameters, this model is, according to Bouchoux *et al.*, universal and can be applied to any colloidal dispersion. In our case, cross-flow shear stress must modify the concentration profile compared to dead-end filtration; but for a formed concentrated layer at steady state with specific Π and k_p , this model may still describe the filtration performance. Therefore, with the first approximation that the concentrated layer in the steady state is no longer affected by the shear flow above this stable deposit of thickness δ , we attempted to predict the localized permeate flux (for each infinitesimal column) along the membrane at steady state based upon this model.

The concentration profiles at steady state were known thanks to SAXS measurements in our case. We then applied Bouchoux' law for each infinitesimal column (z vector) to calculate the localized permeate flux $J(x)$. The equation after integration on the thickness δ of the concentrated layer can be written as

$$J(x) \int_0^\delta cdz = \int_{\Pi_b}^{\Pi_m} \frac{k_p(c)c}{\eta} d\Pi(c) \quad \text{Eq. 3a}$$

Or

$$J(x) \int_0^\delta \phi dz = \int_{\Pi_b}^{\Pi_m} \frac{k_p(\phi)\phi}{\eta} d\Pi(\phi) \quad \text{Eq. 3b}$$

With Π_m and Π_b the osmotic pressure at the membrane surface and at bulk, respectively. Eq. 3 is the equation used in the present paper to obtain $J(x)$ for any infinitesimal boxes (columns) in Fig. 3. All the integral terms are estimated through graphical method.

2.3.4.2 Concentration dependence of Π and k_p

The laws of $k_p(c \text{ or } \phi)$ and $\Pi(c \text{ or } \phi)$ for investigated suspensions (Laponite dispersions and skim milk) are required to fulfill the modeling. Therefore, we have fitted the corresponding curves reported by several groups, as mentioned below. The fitting curves are presented in Fig. 5.

Permeability of Laponite dispersions has been investigated by Lelièvre [19] with a specific designed device. Ranging from $\phi = 7$ to 13 %, he found that the permeability of Laponite deposit did not change with the addition of tspp especially for the lower concentration range (Fig. 5a). Therefore, a common law was considered for the Laponite dispersions both with and without tspp in our modeling:

$$k_p(\phi) = 6 \cdot 10^{-21} \cdot \phi^{-2.08} \quad \text{Eq. 4}$$

Osmotic pressure of Laponite dispersions has been previously investigated by our group using the method well described by Martin et al. [20]. Again, for the same range of concentration ($\phi = 2$ to 10%), difference between two types of dispersions (with or without tspp) can be neglected considering the experimental error (Fig. 5b). In fact, osmotic pressures of Laponite dispersions have been deeply investigated by Lelièvre. He has shown that Π depends greatly on concentration but the dependence of Π and addition of tspp is low [19]. Consequently, a common law for both dispersions was then considered in our modeling (Eq. 5). This power law is verified on all the range of volume fractions measured in the concentration polarization layers, and has been confirmed by theoretical calculation based on Poisson-Boltzmann theory (fig. 10 of ref [19]).

$$\Pi(\phi) = 1.11 \cdot 10^7 \cdot \phi^{2.26} \quad \text{Eq. 5}$$

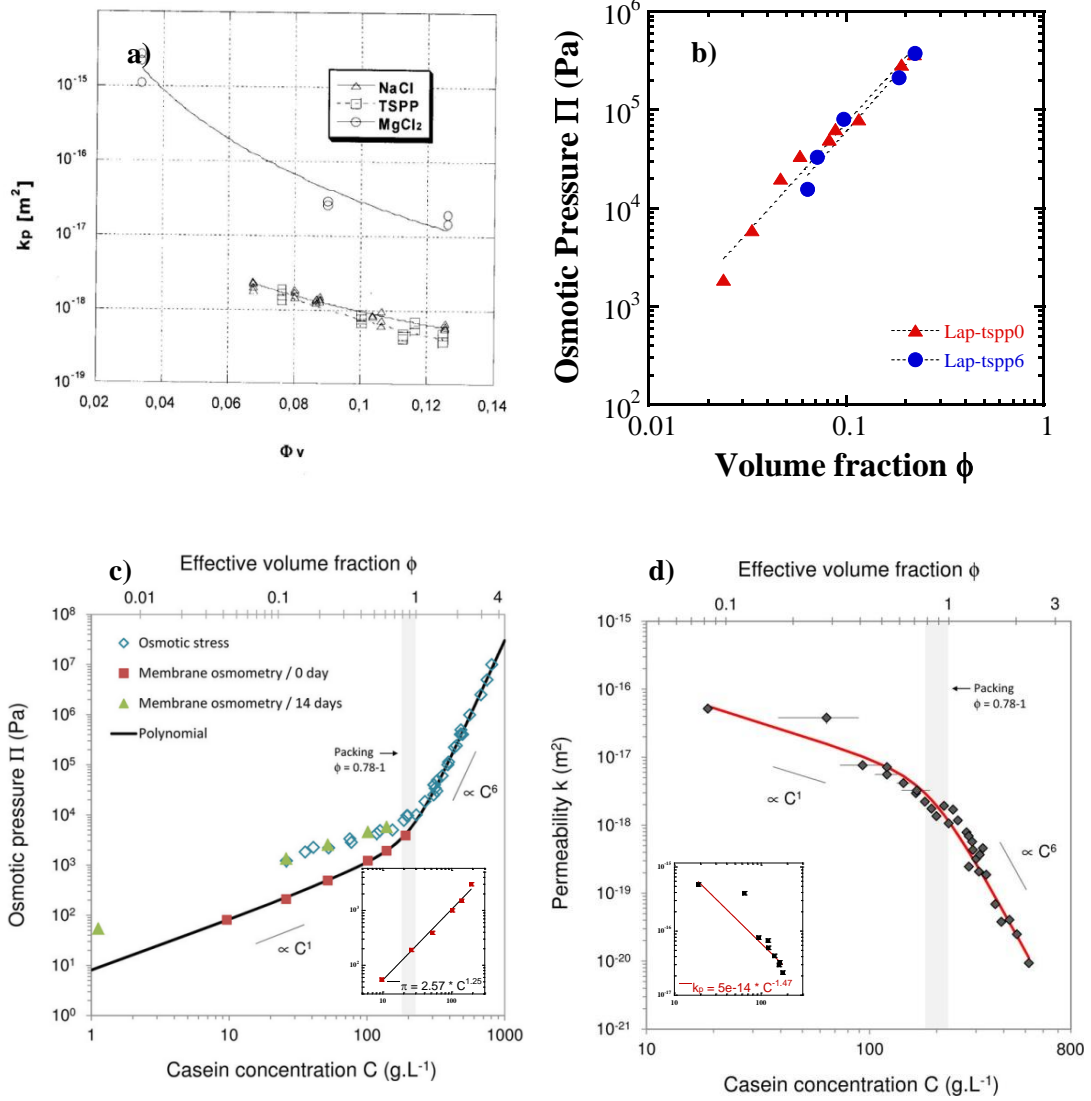


Fig. 5 Laws of permeability and osmotic pressure for Laponite dispersions and casein micelle suspension. a) permeability law of Laponite, captured from [19]; b) osmotic pressure law of Laponite; c) permeability law of casein micelle suspension, captured from [17]; d) osmotic pressure law of casein micelle suspension, captured from [17]. In c and d, the fitting parts used in this paper are presented in the embedded charts.

As for skim milk, concentration dependence laws of these two factors are reported in recent work of Bouchoux [17] for casein micelle suspension (Fig. 5c and d). However, the laws they proposed did not provide us a good prediction of $J(x)$ probably because the empirical laws are dominated by high concentration regime and do not fit well in low concentration regime ($27 \leq C < 200, g.L^{-1}$; $C_0 \leq C < 7.35 * C_0$) where our results are positioned. Therefore, we refit their data in low concentration regime and we obtained:

$$k_p(C) = 5.10^{-14} \cdot C^{-1.47}, C < 200 g.L^{-1} \quad \text{Eq. 6}$$

$$\Pi(C) = 2.57 \cdot C^{1.25}, C < 200 \text{ g} \cdot \text{L}^{-1}$$

Eq. 7

3 Results and discussions

As mentioned before, four key factors of the buildup of concentrated layer are investigated in this paper: matter accumulation, flow property, permeability and osmotic pressure. This section presents some interesting results of each factor and the attempts to correlate each of them with the filtration performance.

3.1 Matter accumulation of concentrated layer

Sourced from Ref.[12], followed by the numerical treatments as described in section 2.3.1 and 2.3.2, the concentration profiles obtained by *in-situ* SAXS measurements have been converted into the corresponding profiles of matter accumulation. Fig. 6 and Fig. 7 demonstrate respectively the mass of concentrated layer along x axis for skim milk suspensions at feed concentration of C_o and $2 \cdot C_o$. They are presented the same way as Ref.[12]: by operational steps.

3.1.1 Feed concentration of C_o

During filtration of skim milk at C_o (Fig. 6), two cross-flow rates ($Q_v = 0.3$ and $0.1 \text{ L} \cdot \text{min}^{-1}$) were applied and US was added for a given duration after steady state was reached. These different conditions divided the filtration run into 4 steps, as presented in Fig. 6e. Reduction of Q_v from 0.3 to $0.1 \text{ L} \cdot \text{min}^{-1}$ resulted in a double mass accumulation, from step 1 to 2 (see Figure a and b). A good coherence between mass accumulation and permeate flux is obtained since J_v dropped off by 2 times from step 1 to 2. Moreover, the additional particles were attributed rather downstream than upstream, which can be observed clearly by comparing these two curves (Figure d). It implies that the axial dependent particle layer deposition was respected all the time during these two steps of filtration. This spatial distribution of matter accumulation along the membrane surface have been predicted in the past by numerous theoretical predictions and modeling of the concentration polarization layer [1-10,15-16], but thanks to the local approach of *in-situ* SAXS measurements, it was the first time that this spatial distribution was experimentally characterized *in-situ* and in the vicinity of the membrane surface from $20 \mu\text{m}$ to few hundred of μm above the membrane surface, with an accuracy of $20 \mu\text{m}$. This accumulated spatial distribution along the membrane has allowed to determine the total mass accumulation of colloids along the entire membrane and offer the possibility to calculate the permeation flux with the model described in part 2.

At the end of step 2, US was applied at step 3, as discussed in Ref.[12], it could not remove this concentrated layer but it brought about a reduction of matter accumulation (see Figure b and c). We have shown that it was difficult to remove the accumulated layer by US once it was formed during filtration of skim milk. In addition, total mass accumulation of step 3 was slightly higher than that of step 1 (2.09 VS 1.82 mg), which corresponds to a slightly lower permeate flux J_v (5.2 VS 4.5 L.h⁻¹.m⁻²). At step 4, US was switched off, the operating conditions were the same as step 2. As shown in Figure d, mass profile is also the same as step 2, which suggests that effect of US was instantaneous in this situation and its effect completely reversible.

3.1.2 Feed concentration of 2*C_o

In a second experiment with an initial filtration concentration of skim milk at 2*C_o (Fig. 7), US was applied before filtration (preventive mode) at step 1. The results shown that profiles of both upstream (x = 7 mm) and downstream (x = 93 mm) were slightly thicker and more concentrated than midstream. Consequently, a U-shape mass profile is revealed, as illustrated in figure a. US seem to be more efficient in disrupting the concentrated layer in the middle of the filtration cell than the two other positions. This can be explained by the fact that the ultrasonic power is relatively higher in the middle of the channel than the two ends where amplitude loss is more pronounced [20]. Stronger ultrasonic activity then results in the disruption of concentrated layer more marked in the middle of the filtration cell.

At step 2, when US was switched off, matter accumulation has increased (see Fig. 7d). From step 1 to 2, J_v declines by 60 % (from 8.3 to 3.3 L.h⁻¹.m⁻²) while accumulated mass increases only by 20 % (from 3.19 to 3.88 mg). Furthermore, mass profile still exhibits U-shape form as step 1 even without US.

Now considering all the three mass profiles presented in Fig. 7, it has been shown that the U-shape form was conserved whatever the different successive filtration conditions with or without US. It was then filled with more particles at step 2 and dug out at step 3. This phenomenon implies that one part of the accumulated protein layer is stagnant in this condition and has a mechanical resistance sufficiently high to resist at shear forces induced by the cross flow. It consolidates the remarks we gave in Ref.[12] that there is a cohesive layer on the membrane surface and increase of feed concentration may strengthen this layer in an important extent.

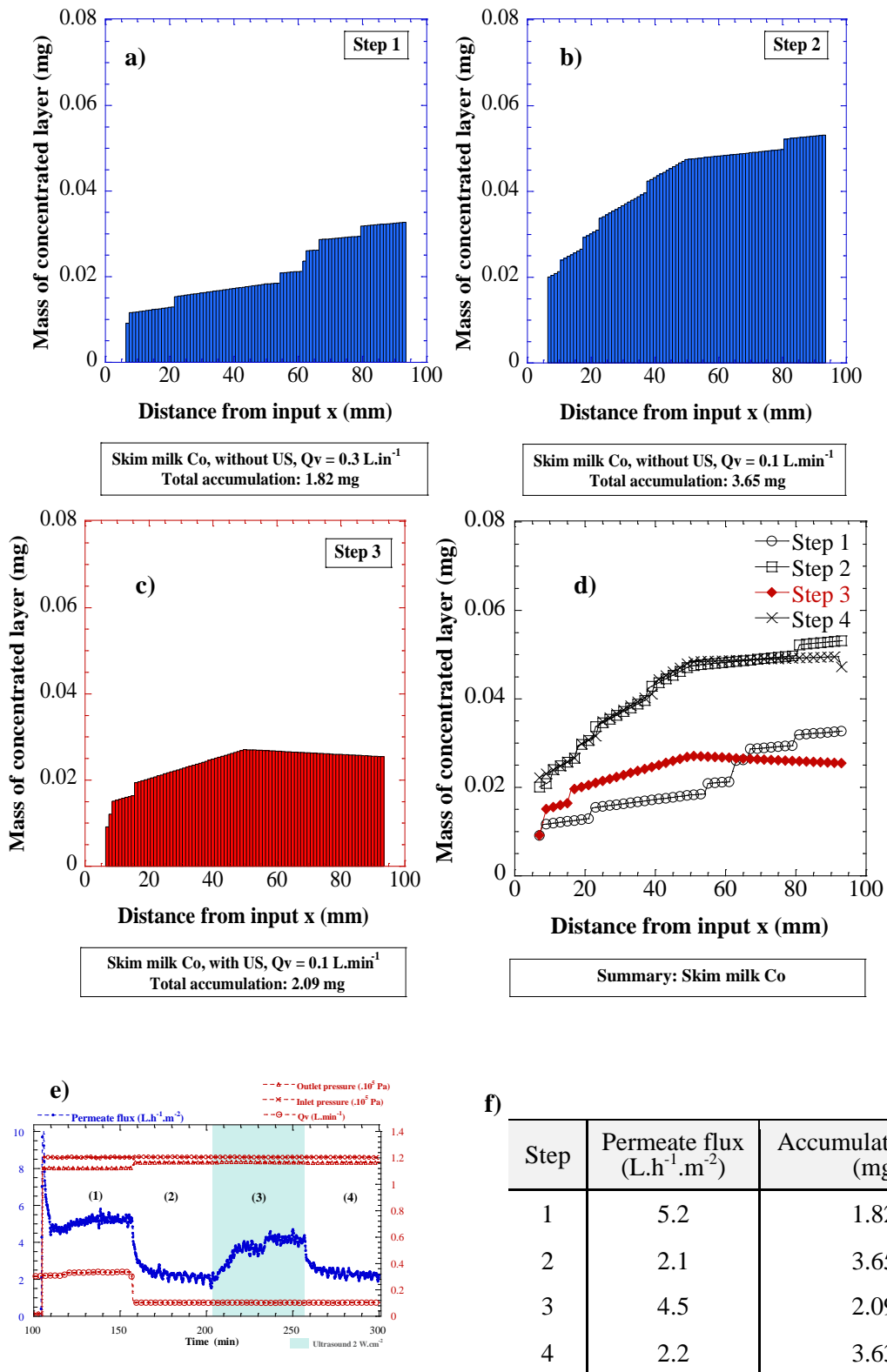


Fig. 6 Matter accumulation of concentrated layer along x axis during filtration of skim milk suspensions (feed: C_o). $T = 25 \pm 1^\circ\text{C}$, $\text{TMP} = 1.1 \times 10^5 \text{ Pa}$. US: 20 kHz, $2 \text{ W}\cdot\text{cm}^{-2}$. a-d: mass profiles; e: reminder of permeate flux J_v curve for step 1 to 4; f: table of values for each step at steady state.

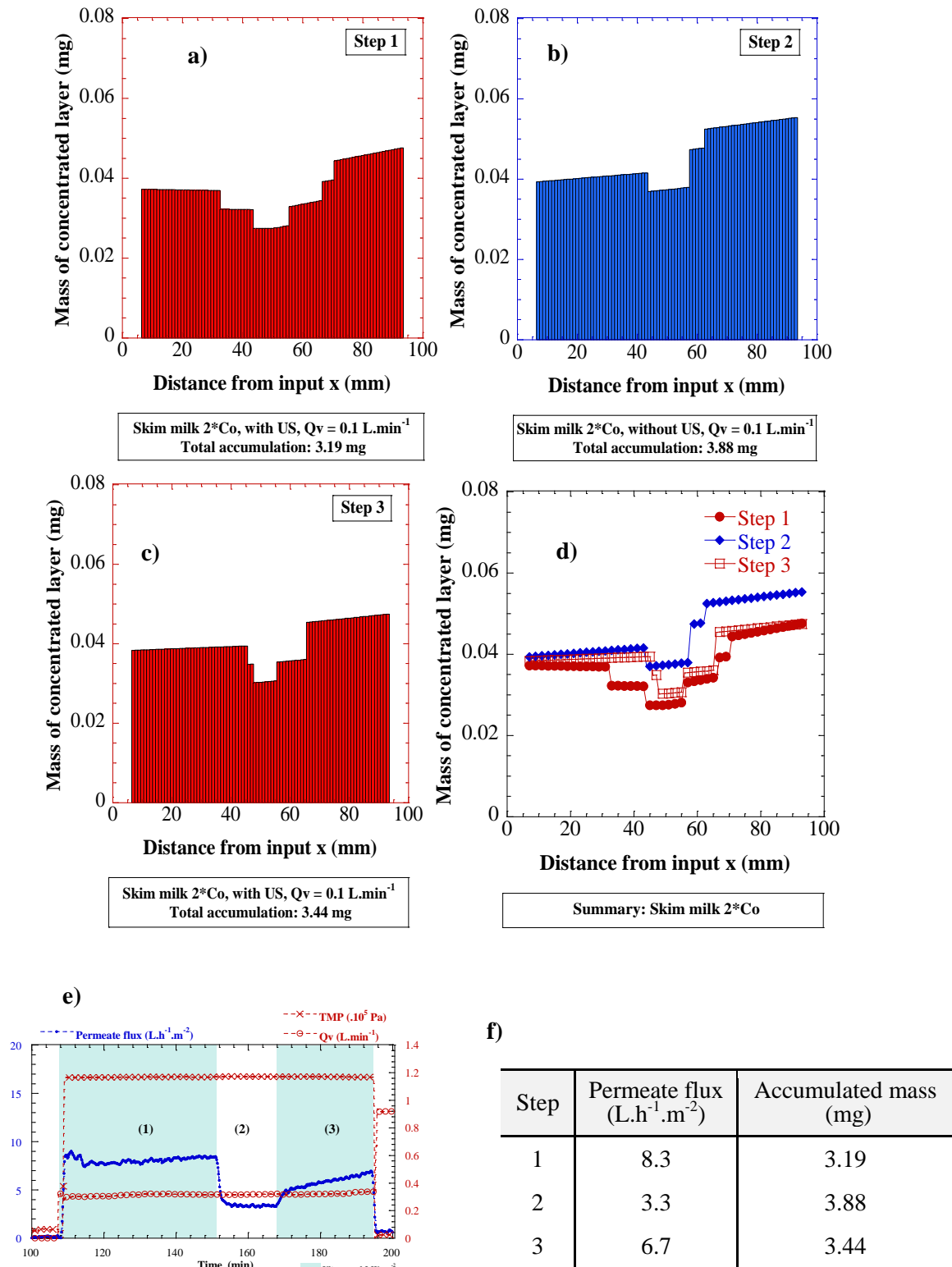


Fig. 7 Matter accumulation of concentrated layer along x axis during filtration of skim milk suspensions (feed: 2^*C_o). $T = 25 \pm 1^\circ\text{C}$, $\text{TMP} = 1.1 \times 10^5 \text{ Pa}$. US: 20 kHz, $2 \text{ W}\cdot\text{cm}^{-2}$. a-d: mass profiles; e: reminder of permeate flux J_v curve for step 1 to 3; f: table of values for each step at steady state.

3.1.3 Correlation between matter accumulation and permeate flux

In order to evaluate the correlations between matter accumulation and permeation flux, all the results obtained in the previous section was summarized in Fig. 8 including the results of both skim milk and Laponite dispersions (feed $\phi = 1\%$) under different operating conditions. Certain correlation between matter accumulation and permeate flux for a given suspension were obtained but a general trend could not be extracted from this set of data on different kind of colloidal particles. These results comfort the fact that other factors such as flow property, permeability k_p and osmotic pressure Π of accumulated layer can also play an important role in this process. It will further be discussed in the next section of this paper.

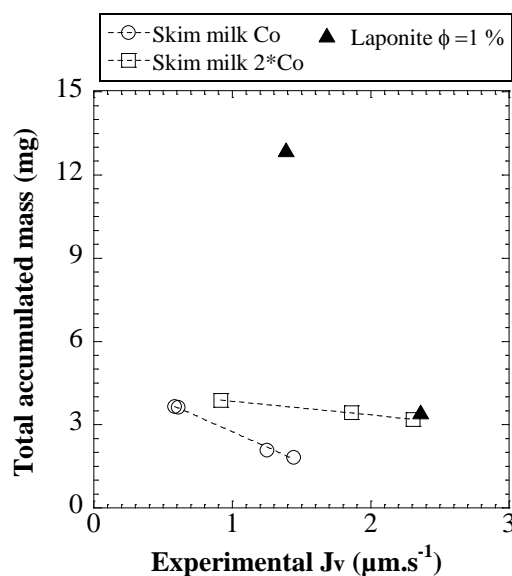


Fig. 8 Correlation between total accumulated mass (calculated from the concentration profiles deduced by in-situ SAXS) and averaged permeate flux for different suspensions.

3.2 Flow properties of concentrated layer

In US assisted cross-flow filtration process, colloidal suspensions are constantly subjected to shear stress, thus their flow properties are crucial for understanding their filtration performance. As shown in our previous work [14], US effect on concentrated layer was extremely different for Laponite dispersions of the same concentration with or without tspp: the applied US induced a removal of accumulated layer in the case of Lap-tspp6 while no change of concentrated layer was detected by the employed SAXS measurement. For both cases, US brought about a great increase of permeate flux.

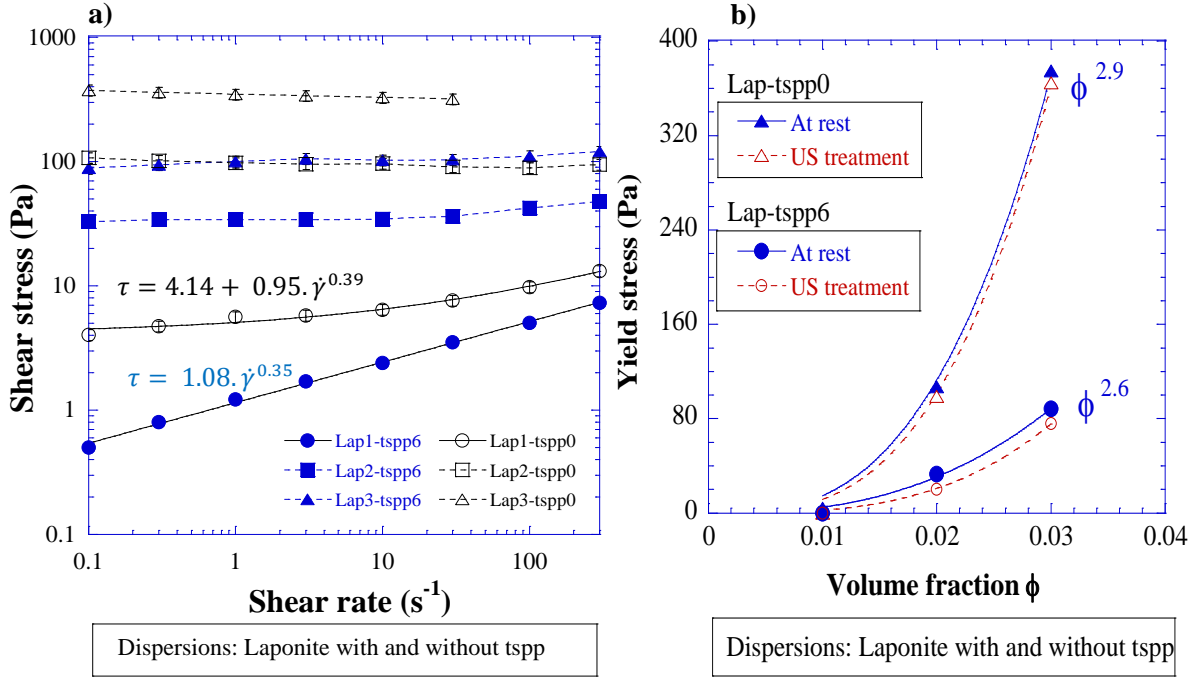
In order to emphasis the effect of flow properties on concentrated layers' formation during filtration, the rheological properties of Laponite dispersions were studied as a function of volume fraction and

mutual inter particle interactions by the addition of peptizer. The obtained results detailed thereafter (Fig. 9) have shown that the flow properties of Lap-tspp0 and Lap-tspp6 are extremely different arising from the mechanical resistance of particle network. First of all, steady-state flow properties of Laponite dispersions without peptizer (Lap-tspp0) and with peptizer (Lap-tspp6) were revealed in Fig. 9a, presenting the measured shear stresses (τ) in steady shear flows. These curves show the influence of volume fraction and addition of peptizer on the shear stresses of the dispersions when a constant shear rate ($\dot{\gamma}$) is applied.

It appears that dispersions containing no peptizer follow the stress curves with a stress plateau (unfilled symbols). As already discussed in literature [21-22], the stress levels at very low shear rates tend towards a yield stress value corresponding to the dynamic yield stress of the gelled dispersions. Addition of peptizer reduces this dynamic yield stress, as shown in Fig. 9a (filled symbols). These results indicate that the network of mechanical links of pure Laponite dispersions has been weakened or dissociated by the addition of peptizer.

Non-Newtonian flow behaviors can be described by power law or Herschel-Bulkley law. Two curves of $\phi = 1\%$ have been fitted by these laws, presented by the solid lines in Fig. 9a. Yield stress of Lap1-tspp0 has been revealed while there is no yield stress for Lap1-tspp6. For this low volume fraction of 1 %, the strain field is homogeneous in the wall gap of the tools and no slip at the wall or localization phenomena have been observed. As volume fraction rises beyond 1 %, the steady stress levels remain quite constant, thus neither of the two laws is capable to describe such behavior perfectly. This phenomenon is associated with a particular mode of deformation, in which all shear is localized in a thin layer of the sample [22]. In this case, the values of shear stress at lowest apparent shear rate of this investigation ($\dot{\gamma} = 0.1 \text{ s}^{-1}$) were considered as the estimated yield stresses of correspondent samples. The estimated yield stresses for these 6 samples are presented in Fig. 9b by filled symbols.

In addition, the samples subjected to US treatment (as described in section 2.3.3) have been characterized by the same procedure. Their estimated yield stresses are presented in Fig. 9b by unfilled symbols, corresponding values are shown in Tab. 1. The applied US treatment reduced the yield stress of all concerned samples (from 2.6 % to total removal, Tab. 1). The reduction is more important for Laponites with peptizers whose yield stresses are much lower than those without peptizer. It suggests that Laponite dispersions with peptizers (6%) are more susceptible to ultrasonic force than those without peptizer, resulting from the reduction in attractive forces between the particles. This difference in behavior should have some consequences on the particle accumulation near the membrane surface during the ultrafiltration process. It is therefore interesting to determine yield stress charts within the filtration channel for both of them to illustrate what happened during this process, with the yield stress/volume fraction dependences obtained from Fig. 9b.



Affiliated table: curve fitting

Dispersion	Law of yield stress (τ_o)/volume fraction (ϕ) dependence
Lap-tspp0	$\tau_o = 1.12 \cdot 10^7 \cdot \phi^{2.94}, 0.01 \leq \phi \leq 0.03$ <i>Eq. 8</i>
Lap-tspp6	$\tau_o = 8.50 \cdot 10^5 \cdot \phi^{2.61}, 0.01 < \phi \leq 0.03$ <i>Eq. 9</i>

Fig. 9 a) Steady-state flow curves of Laponite dispersions at different volume fractions and at different peptizer concentrations without treatment. $T = 25 \pm 1$ °C, $t_p = 12$ days. Solid lines represents curve fitting by power law or Herschel-Bulkley law. b) Yield stress/volume fraction dependence of Laponite dispersions. $T = 25 \pm 1$ °C, $t_p = 12$ days. Solid lines represents curve fitting by appropriate law, the outcome are presented in affiliated table.

Tab. 1: Comparison of yield stress values between “at rest” and “US treatment” of Laponite dispersions

ϕ	Dispersion	τ_o (Pa)		
		At rest	US treatment	Variation
3 %	Lap-tspp0	374.7	364.8	-2.6%
	Lap-tspp6	88.2	76.0	-13.8%
2 %	Lap-tspp0	107.3	99.0	-7.7%
	Lap-tspp6	32.9	20.2	-38.6%
1 %	Lap-tspp0	4.1	/	-100%
	Lap-tspp6	10^{-4} *	/	/

*There is no detected yield stress for Lap-tspp6 at $\phi = 1$ %. In order to have a power law fitting as Lap-tspp0, an approximation treatment was carried out: 10^{-4} Pa was given instead of 0 Pa.

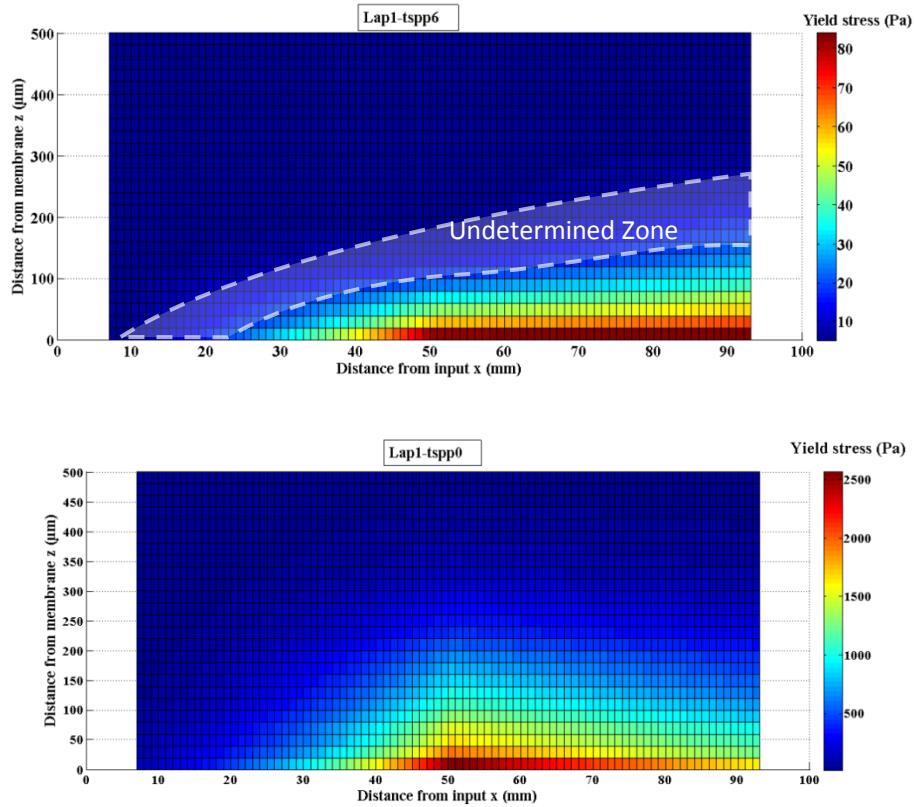


Fig. 10 Charts of yield stress during filtration of Laponite dispersions. a) Lap1-tspp6, b) Lap1-tspp0. Operating conditions: steady state, $T = 25 \pm 1^\circ\text{C}$, $\text{TMP} = 1.1 \times 10^5 \text{ Pa}$, $Q_v = 0.3 \text{ L.min}^{-1}$.

Fig. 10 shows the yield stress charts of Lap1-tspp6 (a) and Lap1-tspp0 (b) within the filtration channel when US was not applied. These two dispersions were filtrated under the same operating conditions. It should be noted that there is an undetermined zone for Lap-tspp6 (Fig. 10a), since we carried out the approximation treatment when determining the τ_o/ϕ law (replacing 0 Pa by 10^{-4} Pa). In fact, the emergence of yield stress for Lap-tspp6 should be between 1 % and 2 %, therefore, our applied law overestimated the yield stress values at the range of [1%, 2%]. Nevertheless, an interesting point is revealed by Fig. 10: yield stress of concentrated layer at the membrane interface does not exceed 100 Pa for Lap1-tspp6 while it can reach around 2500 Pa maximum for Lap1-tspp0. Reminding that contrary to Lap1-tspp6, removal of the concentrated layer of Lap1-tspp0 was not detected under US during filtration [14]. We speculate that gel consistency of concentrated Lap1-tspp0 was so high that the shear stress induced by US was incapable to break up its network, while yield stress of concentrated Lap1-tspp6 was within the capacity of the applied US so that its network was broken up.

This speculation can also explain the quick removal of concentrated layer in certain cases. Fig. 11 shows the evolution of concentration profiles within the accumulated particles layer over time during ultrafiltration of Lap0.48-tspp6 under US. Comparison between the profile at 1 min and 4 min indicates that the top, less concentrated part of the accumulated layer was disrupted immediately and the thickness of accumulated layer reduces since the first moment of US application. It can be explained by the fact that the mechanical links between particles within the concentrated layer are so weak (absence of yield stress) at the range of $\phi = [0.48\%, 1\%]$ that the shear stress induced by US can easily break it up, even immediately.

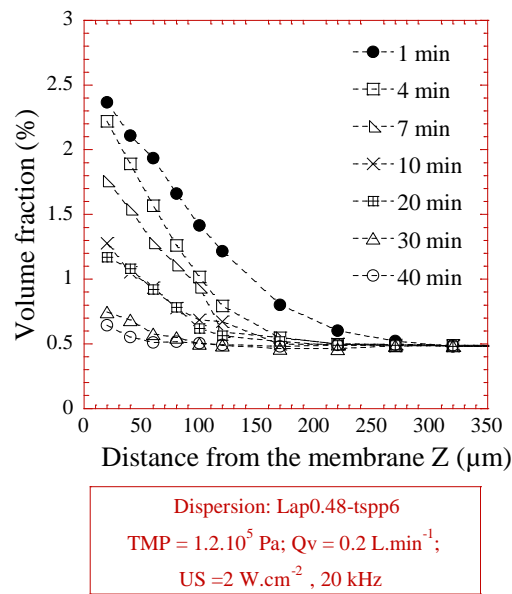


Fig. 11 Evolution of concentration profiles within the accumulated particles layer over time during ultrafiltration of Laponite dispersions (Lap0.48-tspp6, $t_p = 12$ days) with US.

In this section, flow property of concentrated layer has been demonstrated as a relevant factor controlling cross-flow filtration. It provided us valuable explanations especially when the process was subjected to multiple forces (e.x. addition of ultrasonic force).

3.3 Permeability and osmotic pressure of concentrated layer

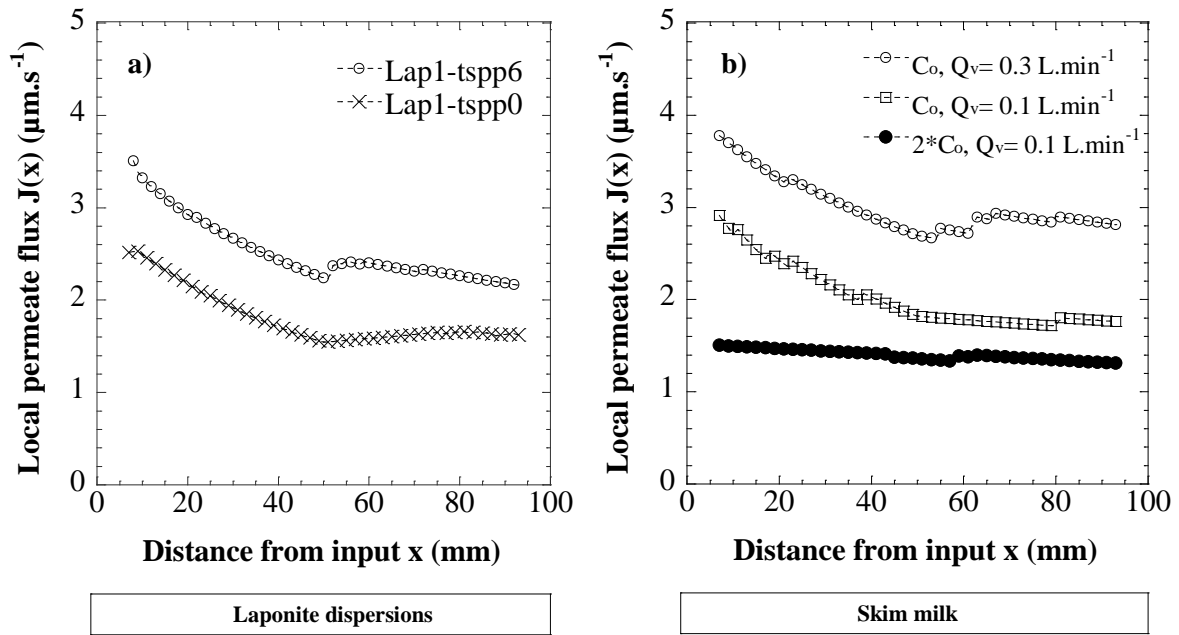
On the basis of the discretized concentration profiles of each case (example described in Fig. 3), model prediction of local permeate flux along x axis $J(x)$ was calculated with Eq. 3 taking into account principally two factors: permeability k_p and osmotic pressure Π of the concentrated layer. This section will present the results from modeling for two types of colloids: Laponite and skim milk. Modeling

will be then assessed by comparing the values of modeled permeate flux with experimental ones. This section will only include the results of filtration without ultrasound.

3.3.1 Modeled local permeate flux along x axis $J(x)$

Fig. 12 presents the permeate flux profiles along the membrane at steady state during filtration of two colloids in 5 different cases. Gathering all the modeled average fluxes of this section, Fig. 13 provides a simple mean to assess the modeling by plotting the values from modeling as a function of experimental ones. Diagonals then stand for the perfect matches that split the charts by two zones: overestimated zone and underestimated zone. First of all, we should emphasize that the modeling approach is satisfactory since all the modeled permeate flux values are in the same order of magnitude of the experimental ones. Then the agreement between modeling and experimental data differs from case to case.

In Fig. 12a, two cases of Laponite dispersions are presented. Both of them exhibit an x axial dependence: higher permeate flux near the inlet than outlet of the channel. It is consistent with the correspondent concentration profiles illustrated before. Again, difference between Lap1-tspp0 and Lap1-tspp6 is revealed: better performance for Lap1-tspp6 with higher average flux (shown in affiliated table). The average of local permeate flux (calculated according to Eq. 3) should match the experimental J_v in ideal situation. In the case of Laponite dispersions, model predictions are slightly overestimated, as shown by unfilled squares in Fig. 13 **Erreur ! Source du renvoi introuvable.** If we plot a fitting curve with the two obtained points (true, more points are required to plot for real), it will be parallel to the perfect match line (diagonal), suggesting that the applied model is capable to predict the process performance for the studied cases.



Affiliated table: average flux

Case	Dispersion	Q_v (L.min ⁻¹)	v (m.s ⁻¹)	Modeled average flux J_v (μm.s ⁻¹)	Experimental average flux J_v (μm.s ⁻¹)
1	Lap1-tspp6	0.3	0.16	2.97	2.36
2	Lap1-tspp0	0.3	0.16	1.81	1.39
3	Skim milk C_o	0.3	0.16	3.00	1.44
4	Skim milk C_o	0.1	0.05	2.02	0.58
5	Skim milk $2*C_o$	0.1	0.05	1.40	0.92

Fig. 12 Permeate flux profile along the membrane, calculated according to Eq. 3. a) Laponite dispersions; b) skim milk. $T = 25 \pm 1^\circ\text{C}$, $TMP = 1.1 \times 10^5$ Pa. The modeled and experimental average fluxes are shown in affiliated table.

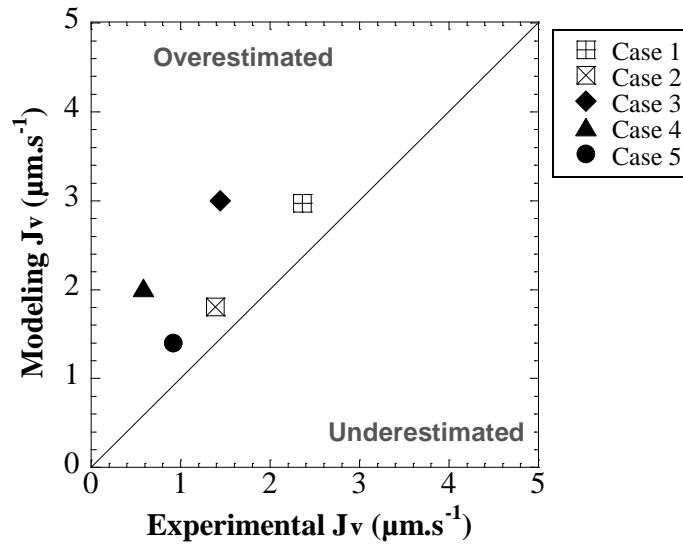


Fig. 13 Comparison of model predictions with experimental results of average fluxes J_v . Diagonals represent the perfect match lines.

The permeate flux profiles for skim milk (feed concentration at C_o and $2*C_o$, $Q_v = 0.1$ or $0.3 \text{ L}\cdot\text{min}^{-1}$) are assembled in Fig. 12b. Both of the decrease of Q_v (from 0.3 to $0.1 \text{ L}\cdot\text{min}^{-1}$) and the increase of feed concentration (from C_o to $2*C_o$) induced a reduction of local permeate flux. Case 5 is actually the steady state result of step 2 in Fig. 7e. Consistent with its mass profile (Fig. 7b), it loses the x axial dependence feature; the difference between upstream and downstream is not pronounced. Overestimation is generally more important in the case of skim milk than Laponite, as shown by the filled symbols in Fig. 13. This overestimation could result from the used laws of k_p and Π in modeling. In fact, the used laws are both empirical for native phosphocaseinate (NPC) dispersions which contain principally casein micelles. Content of whey proteins in this dispersion is much lower than skim milk used in filtration. It implies that the presence of whey protein, which may hamper the permeation of solvent through the network, could affect k_p and Π of concentrated layer resulting in different filtration performance. In addition, concentration at $z = 0 \mu\text{m}$ (membrane surface) was extrapolated by exponential law in the light of obtained concentration information, as shown in Fig. 2b. It needs to be verified by experimental data, using technique as GISAXS [26]. It is possible that the concentration at membrane surface is much higher than the estimated one by extrapolation, which results in the overestimation of permeate flux.

4. Conclusions

Preceding *in-situ* SAXS measurements have allowed to deduce concentration profiles as a function of the distance from the membrane surface but also along the membrane surface during filtration process of two kind of colloidal suspensions composed of hard discs of Laponite clay particles and soft casein

micelles particles. The rheological properties of these colloidal dispersions have been evaluated as a function of concentration, effect of ultrasound and change in inter-particle colloidal forces for Laponite dispersions by the addition of a peptizer. Starting from this set of essential information, a modeling of the filtration properties introducing these experimental data, has been performed in this article in order to evaluate the relationships between the measured and/or calculated permeation flux, and the mechanical and structural properties of accumulated concentrated layers. Several key factors of the concentrated polarization layer formed during such process have been explored: matter accumulation, flow properties, permeability and osmotic pressure of the filtered suspensions.

Matter accumulation within the concentrated layer was calculated from the concentration profiles under different operating conditions. Effects of cross-flow rate and US have been discussed. For all the systems and filtration conditions investigated, the results have shown that the level of matter accumulated is directly linked to calculated permeation flux and in accordance with the measured one.

The rheological parameters of the suspensions introduced in the calculations have allowed to deduce the charts of yield stress in the concentrated layers and has revealed the important role of suspension flow properties in the mechanisms of filtration involved near the membrane surface. Specifically, the great difference of filtration performance among Laponite dispersions with and without peptizer can be well explained by their distinct flow properties. Indeed, the addition of peptizer reduces the strength of interaction between the particles it moves the sol-gel transition to higher volume fraction and reduce the yield stress of the suspension for one volume fraction. For the same filtration conditions, the yield stress of concentrated layer at the membrane interface does not exceed 100 Pa for Laponite with peptizer while it can reach around 2500 Pa maximum for Laponite without peptizer. The consequence of this change in rheological properties is the formation of a thinner and less concentrated layer with peptizer, inducing a higher permeation flux.

Finally, the measured properties of the accumulated layers have been computed with a recent model based upon permeability and osmotic pressure [17]. From the knowledge of permeability and osmotic pressure as a function of the concentration for Laponite [19] and casein micelle suspensions [17], this model has been used to predict the local permeate flux along the membrane surface in the direction of the cross-flow at steady state. This calculated permeation flux has been linked to distribution of the calculated accumulated mass along the membrane surface deduced from the SAXS data. It has been shown good agreement between modeled and experimental values in permeation flux all along the membrane for all the different systems and filtration explored. This highlighted the fact that permeability and osmotic pressure can provide an overall description of filtration performance on these kind of colloidal suspensions.

Acknowledgements

Laboratoire Rhéologie et Procédés is a part of the LabEx Tec 21 (Investissements d'Avenir – grant agreement n° ANR-11-LABX-0030) and of PolyNat Carnot Institut (Investissements d'Avenir – grant agreement no. ANR-11-CARN-030-01).

References

- [1] W.R. Bowen, P.M. Williams, Quantitative predictive modelling of ultrafiltration processes: Colloidal science approaches, *Surf. Forces Wetting Phenom. Membr. Sep. Rheol. Top. Issue Honour Victor Starov*. 134–135 (2007) 3–14.
- [2] M. Elimelech, S. Bhattacharjee, A novel approach for modeling concentration polarization in crossflow membrane filtration based on the equivalence of osmotic pressure model and filtration theory, *J. Membr. Sci.* 145 (1998) 223–241.
- [3] P. Bacchin, D. Si-Hassen, V. Starov, M.. Clifton, P. Aimar, A unifying model for concentration polarization, gel-layer formation and particle deposition in cross-flow membrane filtration of colloidal suspensions, *Chem. Eng. Sci.* 57 (2002) 77–91.
- [4] P. Bacchin, M. Meireles, P. Aimar, Modelling of filtration: from the polarised layer to deposit formation and compaction, *Desalination*. 145 (2002) 139–146.
- [5] P. Aimar, P. Bacchin, Concentrated phases of colloids or nanoparticles: Solid pressure and dynamics of concentration processes, in: *Nanosci. Colloidal Interfacial Asp.*, Victor M. Starov, Taylor Francis Inc, USA, 2010: pp. 1–256.
- [6] W.R. Bowen, Y. Liang, P.M. Williams, Gradient diffusion coefficients — theory and experiment, *Chem. Eng. Sci.* 55 (2000) 2359–2377.
- [7] C. Romero, R. Davis, Global-Model of Cross-Flow Microfiltration Based on Hydrodynamic Particle Diffusion, *J. Membr. Sci.* 39 (1988) 157–185.
- [8] J. Kromkamp, A. Bastiaanse, J. Swarts, G. Brans, R.G.M. van der Sman, R.M. Boom, A suspension flow model for hydrodynamics and concentration polarisation in crossflow microfiltration, *J. Membr. Sci.* 253 (2005) 67–79.
- [9] L. Song, M. Elimelech, Theory of concentration polarization in crossflow filtration, *J. Chem. Soc. Faraday Trans.* 91 (1995) 3389–3398.

- [10] K.J. Martin, D. Bolster, N. Derlon, E. Morgenroth, R. Nerenberg, Effect of fouling layer spatial distribution on permeate flux: A theoretical and experimental study, *J. Membr. Sci.* 471 (2014) 130–137.
- [11] Y. Jin, N. Hengl, S. Baup, F. Pignon, N. Gondrexon, A. Magnin, et al., Effects of ultrasound on colloidal organization at nanometer length scale during cross-flow ultrafiltration probed by in-situ SAXS, *J. Membr. Sci.* 453 (2014) 624–635.
- [12] Y. Jin, N. Hengl, S. Baup, F. Pignon, N. Gondrexon, M. Sztucki, et al., Effects of ultrasound on cross-flow ultrafiltration of skim milk: Characterization from macro-scale to nano-scale, *J. Membr. Sci.* 470 (2014) 205–218.
- [13] Y. Jin, N. Hengl, S. Baup, F. Pignon, N. Gondrexon, M. Sztucki, et al., Ultrasonic assisted cross-flow ultrafiltration of starch and cellulose nanocrystals suspensions: Characterization at multi-scales, *Carbohydr. Polym.* 124 (2015) 66–76.
- [14] N. Gondrexon, L. Cheze, Y. Jin, M. Legay, Q. Tissot, N. Hengl, et al., Intensification of heat and mass transfer by ultrasound: Application to heat exchangers and membrane separation processes, *Sel. Pap. 14th Meet. Eur. Soc. Sonochemistry Avignon Fr. June 2014.* 25 (2015) 40–50.
- [15] Y. Bessiere, D.F. Fletcher, P. Bacchin, Numerical simulation of colloid dead-end filtration: Effect of membrane characteristics and operating conditions on matter accumulation, *J. Membr. Sci.* 313 (2008) 52–59.
- [16] J. Mendret, C. Guigui, C. Cabassud, P. Schmitz, Numerical investigations of the effect of non-uniform membrane permeability on deposit formation and filtration process, *Desalination.* 263 (2010) 122–132.
- [17] A. Bouchoux, P. Qu, P. Bacchin, G. Gésan-Guizieu, A General Approach for Predicting the Filtration of Soft and Permeable Colloids: The Milk Example, *Langmuir.* 30 (2013) 22–34.
- [18] V. Lelièvre, Thèse : Rhéologie et filtration de dispersions aqueuses de nanoparticules d’hectorite en relation avec la structuration des dépôts, INSTITUT POLYTECHNIQUE DE GRENOBLE, Grenoble, 2005.
- [19] C. Martin, F. Pignon, A. Magnin, M. Meireles, V. Lelièvre, P. Lindner, et al., Osmotic Compression and Expansion of Highly Ordered Clay Dispersions, *Langmuir.* 22 (2006) 4065–4075.
- [20] Y. Jin, Thèse: Procédé de séparation membranaire de colloïdes : caractérisation des mécanismes aux échelles nanométriques et intensification par ultrasons, Université Grenoble Alpes, Grenoble, 2014.

- [21] C. Martin, F. Pignon, J. Piau, A. Magnin, P. Lindner, B. Cabane, Dissociation of thixotropic clay gels, *Phys. Rev. E.* 66 (2002) 021401.
- [22] F. Pignon, A. Magnin, J.-M. Piau, Thixotropic colloidal suspensions and flow curves with minimum: Identification of flow regimes and rheometric consequences, *J. Rheol.* 1978-Present. 40 (1996) 573–587.
- [23] Pignon F., Belina G., Narayanan T., Paubel X., Magnin A. and Gésan-Guiziou G., "Structure and rheological behavior of casein micelle suspensions during ultrafiltration process", *J. Chem. Phys.* 121(16) (2004) 8138-8146.
- [24] Marchin S., Putaux J.L., Pignon F. and Léonil J., "Effects of the environmental factors on the casein micelle structure studied by Cryo-TEM and SAXS/USAXS", *J. Chem. Phys.* 126 (2007) 045101.
- [25] T. Narayanan, O. Diat, P. Bösecke, SAXS and USAXS on the high brilliance beamline at the ESRF, *Nucl. Instrum. Methods Phys. Res. Sect. Accel. Spectrometers Detect. Assoc. Equip.* 467–468, Part 2 (2001) 1005–1009.
- [26] R. Gebhardt, U. Kulozik, Simulation of the shape and size of casein micelles in a film state, *Food Funct.* 5 (2014) 780.